AmineFunctionalized Mesoporous Silica Adsorbent for CO2 Capture in ConfinedFluidized Bed: Study of the Breakthrough Adsorption Curves as a Function of Several Operating

Original
AmineFunctionalized Mesoporous Silica Adsorbent for CO2 Capture in ConfinedFluidized Bed: Study of the Breakthrough Adsorption Curves as a Function of Several Operating Variables / Girimonte, R., Testa, F., Turano, M., Leone, G., Gallo, M., Golemme, G.. - In: PROCESSES. - ISSN 2227-9717. - ELETTRONICO. - 10:2(2022), p. 422. [10.3390/pr10020422]

Publisher:
MDPI

Published
DOI:10.3390/pr10020422

processes

Article

Amine-Functionalized Mesoporous Silica Adsorbent for CO_2 Capture in Confined-Fluidized Bed: Study of the Breakthrough Adsorption Curves as a Function of Several Operating Variables

Rossella Girimonte [1,*], Flaviano Testa [1], Maria Turano [1], Giuseppe Leone [1], Marta Gallo [2] and Giovanni Golemme [3]

[1] Dipartimento di Ingegneria Informatica, Modellistica, Elettronica e Sistemistica—DIMES, Università della Calabria, 87036 Rende, Italy; flaviano.testa@unical.it (F.T.); maria.turano@dimes.unical.it (M.T.); leonegiuseppe90@libero.it (G.L.)
[2] Dipartimento di Scienza Applicata e Tecnologia, Politecnico di Torino, 10129 Torino, Italy; marta.gallo@polito.it
[3] Dipartimento di Ingegneria dell'Ambiente—DIAm, Università della Calabria, 87036 Rende, Italy; giovanni.golemme@unical.it
* Correspondence: rossella.girimonte@unical.it; Tel.: +39-0984-496689

Abstract: Carbon capture, utilization, and storage (CCUS) is one of the key promising technologies that can reduce GHG emissions from those industries that generate CO_2 as part of their production processes. Compared to other effective CO_2 capture methods, the adsorption technique offers the possibility of reducing the costs of the process by setting solid sorbent with a high capacity of adsorption and easy regeneration and, also, controlling the performance of gas-solid contactor. In this work, an amine-functionalized mesoporous sorbent was used to capture CO_2 emissions in a confined-fluidized bed. The adoption of a confined environment allows the establishment of a homogeneous expansion regime for the sorbent and allows to improve the exchange of matter and heat between gas and solid phase. The results illustrate how the different concentration of the solution adopted during the functionalization affects the adsorption capacity. That, measured as mg of CO_2 per g of sorbent, was determined by breakthrough curves from continuous adsorption tests using different concentrations of CO_2 in air. Mesoporous silica functionalized with a concentration of 20% of APTES proves to be the best viable option in terms of cost and ease of preparation, low temperature of regeneration, and effective use for CO_2 capture.

Keywords: CO_2 capture; amine-functionalized adsorbents; confined-fluidized bed; CO_2 adsorption

check for updates

Citation: Girimonte, R.; Testa, F.; Turano, M.; Leone, G.; Gallo, M.; Golemme, G. Amine-Functionalized Mesoporous Silica Adsorbent for CO_2 Capture in Confined-Fluidized Bed: Study of the Breakthrough Adsorption Curves as a Function of Several Operating Variables. *Processes* **2022**, *10*, 422. https://doi.org/10.3390/pr10020422

Academic Editors: Federica Raganati and Paola Ammendola

Received: 27 January 2022
Accepted: 18 February 2022
Published: 21 February 2022

1. Introduction

The long-term effects of climate change, including further ice melt, ocean warming, sea-level rise, and ocean acidification, are determined primarily by anthropogenic CO_2 emissions of the last century: a problem that requires an urgent solution. There are various alternatives to reduce greenhouse gas emissions and, in particular, CO_2: reducing the consumption of fossil sources, increasing energy efficiency, using renewable sources or nuclear energy. These widely recognized solutions, however, involve a radical change in energy policies, which therefore require a long period of implementation. Due to the widespread use of fossil fuels for energy production, several techniques are currently developed to eliminate CO_2 emissions in the medium term, grouped together under the terms carbon capture and storage (CCS) and carbon capture utilization and storage (CCUS) [1].

The current techniques for CO_2 capture include physical and chemical absorption, membrane separation, and adsorption. Although absorption is an effective technology, it is costly due to the high energy consumption for solvent regeneration [2].

Instead, adsorption techniques offer the possibility of reducing the costs of the process [3]. However, their feasibility depends mainly on the availability of adsorbents endowed with desirable features: high working capacity, fast kinetics, high CO_2 selectivity, mild desorption conditions, adsorption-desorption stability, tolerance to impurities, and low cost [4].

Among the various options for low-temperature CO_2 removal (e.g., carbons, zeolite, metal-organic framework (MOFs)-based adsorbents) [5–15], amines supported on porous solids have been identified as promising materials due to a loading capacity comparable to the one of liquid amines, acceptable kinetics, high selectivity, simple synthesis and enhanced adsorbing capacity in the presence of water in comparison to the conventional adsorbents [5].

Inorganic mesoporous materials (such as silica) are convenient for this purpose thanks to their large and accessible pore volume that allows for the grafting of amines without significant reduction in CO_2 mobility. In addition, they are mechanically and thermally stable in the presence of low-temperature post-combustion gases [7]. Such support can accommodate the amine molecules, combining the high affinity of amines to CO_2 with the high surface area of a porous adsorbent [6].

Both zeolites and MOFs have a high CO_2 capture capacity, and some of them are quite stable but usually expensive. The polarity and the presence of pores make the zeolite an efficient shape-selective sorbent for a broad range of separation applications.

Several studies about CO_2 capture with mesoporous silicas have been reported in the literature, including MCM-41 [16], MCM-48 [17], SBA-15 [18]. Thanks to the high specific surface area and the high pore volume, these supports can provide more active sites for the reaction of amines with CO_2. SBA-15 is one of the most interesting materials due to its simple preparation, high stability, and the presence of micropores interconnecting its meso-channels, which contribute to gas physisorption [19].

Recently, organic amine-modified SBA-15 solid adsorbent has become one of the research hotspots in the field of CO_2 capture, thanks to the regular open-framework structure and pore size, high specific surface area, and high hydrothermal stability. Leal et al. reported CO_2 adsorbing reversibly on a silica gel containing 3-aminopropyl groups bonded to surface silanols [20]. Zhao et al. studied CO_2 adsorption on TEPA functionalized mesoporous SBA-15. It was found that all the impregnated SBA-15 sorbents showed reversible carbon dioxide adsorption behaviors with fast adsorption kinetics [21]. To improve the performance of the adsorbent, Zheng et al. modified SBA-15 by ethylenediamine (EDA) and prepared the EDA-SBA-15 adsorbent. This EDA-SBA-15 adsorbent is relatively stable below 20 °C and can realize complete desorption of adsorbed CO_2 below 110 °C [22]. The adsorption performance was insensitive to humidity. Zhou et al. added Zr (IV) ions and trimethylbenzene (TMB) into the traditional synthetic SBA-15 solution and synthesized one flake-like SBA-15 with short pore pathways and a large pore diameter. After organic amine was loaded into SBA-15, the N_2 content was 66% higher and the CO_2 adsorption 120% higher compared to those in traditional fibrous SBA-15 [23]. In amine-functionalized adsorbents, the homogeneous dispersion of the amine is an important factor for CO_2 adsorption. To increase amine dispersity, Sanz-Perez et al. added aminopropyl-trimethoxysilane (AP) during absorbent preparation [24]. Under 45 °C and 0.1 MPa, the CO_2 adsorption was 2.4 mmol/g and the corresponding use of amine 0.32. To load more amine into the carrier, Jung et al. prepared the absorbent 1N-SG/TEPA-30 by the dipping method. Its CO_2 adsorption capacity reached 2.64 mmol/g and the use of amine 0.31 [25]. Yue et al. increased dispersity of amine by using SBA-15(P) containing the template P123 as the carrier and increased concentration of hydroxyl groups on the solid adsorbent surface by the mixed loading of TEPA and hydramine, which could increase further the CO_2 adsorption capacity [26,27].

Functionalization of the porous materials with amines can be carried out by impregnation or by grafting. Impregnation is usually performed by loading amine polymers in the pore volume, while grafting is based on the condensation reaction between surface silanol groups and the products of hydrolysis of the amino-silane molecules [28]. Some of the amine molecules used for impregnation in the literature are polyethyleneimine (PEI) [29], tetraethylenepentamine (TEPA) [30], monoethanolamine (MEA), diethanolamine (DEA), pentaethylenehexamine (PEHA), while 3-aminopropyltriethoxysilane (APTES) and other aminoalkoxysilanes are used for grafting purposes [31–33].

In Figure 1, a simplified mechanism of CO_2 capture is depicted. Physisorption occurs on the surface of silica particles by interaction with silanol (Si-OH) groups, while chemisorption occurs through reaction with the grafted -NH_2 groups.

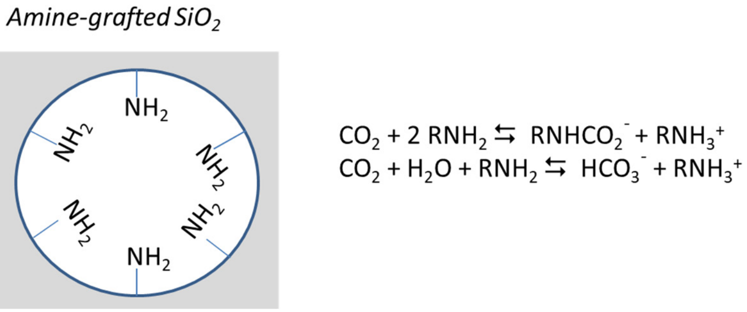

Figure 1. Mechanism of CO_2 capture over amine-modified silica.

For amine-functionalized supports, CO_2 uptake is expected to occur mainly by chemisorption at low partial pressure of CO_2. The introduction of various amine-containing basic moieties, for instance, into porous solid sorbents is found advantageous to markedly strengthen their capture capacity. In fact, interaction with CO_2 via chemical leads to the formation of carbamates and bicarbonates when CO_2 reacts with amine-groups in anhydrous and hydrous conditions, respectively. It has been widely reported that the CO_2 uptake by solid amine-based systems increases in the presence of H_2O because of the formation of bicarbonates [34].

In this work, a commercial silica gel has been tested as a CO_2 sorbent from CO_2-air mixtures that simulated post-combustion concentration conditions after being amino-functionalized. In particular, the main operating variables affecting the adsorption capacity have been investigated (amount of amino groups on silica, CO_2 concentration of the processed mixture, and layout of the gas-solid contact). Before the TSA experimental campaign, the sorbent has been fully characterized from the chemical-physical and fluid-dynamic points of view. In a previous study [35], two of three samples here compared had been already tested. In this work, the new results on the sample prepared with the lowest concentration of APTES are added in order to optimize the effect of the amount of –NH_2 groups on the adsorption capacity. Then, a systematic campaign of adsorption experiments has been carried out on the best sample at different CO_2 concentrations (5%–20%) in the air stream, both in conventional and in confined-fluidized beds at comparable values of gas velocity, to reveal the improved performance of the confined layout.

2. Materials and Methods

2.1. Materials

Commercial silica gel (Davisil® Grade 636) was used as the sorbent. Silica and 3-aminopropyltriethoxysilane (APTES, >98%) were provided by Sigma-Aldrich (St. Louis, MO, USA). Ethanol (96%, analysis grade) was provided by J.T. Baker-Avantor (Radnor, PA, USA).

A 400–500 µm silica sample was prepared by sieving to obtain a sample with a short granulometric dispersion, and, before the adsorption tests, it was characterized using several characterization techniques.

2.2. Characterization Methods

Particle size distribution was determined by a Helos laser diffractometer (Sympatec GmbH, Clausthal-Zellerfeld, Germany), and particle shape was characterized with a QicPic image analysis system (Sympatec GmbH, Clausthal-Zellerfeld, Germany). The average volume diameter was 0.527 mm with a value of sphericity of 0.75 [35]. The grafting with APTES did not change the particle average diameter, but it modified particle density.

Nitrogen adsorption-desorption isotherms at 77 K were acquired using an ASAP 2020 Plus analyzer and a TriStar II 3020 (Micromeritics, Norcross, GA, USA). The specific surface area (S_{BET}), total pore volume, pore size, and particle density were calculated and estimated by referring to previous work [35].

Micrographs were obtained by means of a Merlin SEM (Zeiss Instruments, Oberkochen, Germany) [35].

X-ray diffraction (XRD) spectra were collected using a MiniFlex 600 from Rigaku in the 2θ range between 0.7° and 60°, with steps of 0.02 deg and a speed rate of 4 deg/min.

The thermogravimetric analysis (TGA) was performed using a DSC-TGA STA 409C analyzer (Netzsch-Gerätebau GmbH, Selb, Germany) from 20 to 800 °C at a heating rate of 10 deg/min in static air.

Fluid-dynamic characterization of the sorbent was carried out by fluidization experiments in a conventional and confined environment.

2.3. Preparation of APTES-Grafted Mesoporous Silica

To verify the effect of the functionalization degree, amino groups were grafted on silica using ethanol/water solutions having different concentrations of APTES (10%, 20%, 40% *w*/*w*), according to a modified procedure reported by Quang et al. (2016) [36].

In a typical experiment, 100 g of silica gel were dried in an oven at 120 °C for 2 h, soaked with 400 g of APTES solution for 72 h at room temperature, and, successively, for 48 h at 40 °C under mechanical stirring. Finally, the slurry was dried in an oven at 60 °C for 48 h.

2.4. Experimental Apparatus and Procedure for the Adsorption Tests

The experimental campaign was carried out in a laboratory-scale fluidization column made of plexiglass, with an internal diameter of 50 and 700 mm high. Detailed description of the apparatus was given in reference [35]. For confined fluidization, first, the glass beads that act as a filling were loaded into the column for a height of 450 mm. Then the adsorbent solid percolates into the empty interstices created by the packing. The gas used for fluidization of the fine adsorbent bed was air, whose flow rates were regulated by a set of rotameters covering the range 10–1600 Nl/h.

The dynamic CO_2 adsorption tests have been carried out in beds of different samples with CO_2/air gas mixtures. From the compressor, the air is put in a column for the humidity abatement and mixed at a prefixed flow rate of CO_2 coming from the cylinder. To verify the desired CO_2/air composition, the mixture is intercepted by the three-ways valve, which allows the column to be bypassed and switched to a gas analyzer (GA-21 plus—Madur Polska Sp. Z o.o., Zgierz, Poland). Through the same three-ways valve, the mixture is finally switched inside the column, and the outlet concentration of CO_2 is now measured by the gas analyzer and acquired on a computer.

The measurements allow obtaining breakthrough curves and their parameters: the breakthrough time, the saturation time, the fraction of bed used at the breakpoint, and the adsorption capacity measured as mg of CO_2 per g of sorbent [37].

After each cycle of adsorption, the sorbents were regenerated by static heating in an oven at 120 °C: a TGA analysis after three and nine cycles of adsorption/desorption had shown the high level of thermal stability of the samples, in particular of APTES20 [35].

3. Results and Discussion

3.1. Results of the Adsorbent Characterization

Particle apparent density of the porous adsorbent was determined according to the method proposed by Abrahamsen and Geldart (1980) and explained comprehensively in previous works [35,38]. In this case, siliceous sand of density ρ = 2660 kg/m^3, used as a reference, was loaded into a graduated cylinder and compacted until a value of minimum voidage of 0.457. This value applied to three functionalized samples resulted in higher values of particle density, as indicated in Table 1.

Table 1. Particle density, Brunauer–Emmett–Teller (BET) specific surface, and Barrett–Joyner–Halenda (BJH) pore volume of the adsorbent particles.

Adsorbent	ρ (kg/m^3)	S_{BET} (m^2/g)	Pore Volume (cm^3/g)	Pore Size Range (nm)	Ref.
As-made Silica	947	584	0.89	3–20	[35]
APTES10	1020	264	0.70	3–19	This work
APTES20	1380	180	0.30	3–15	[35]
APTES40	1520	73	0.10	3–13	[35]

The N_2 adsorption/desorption isotherms at 77 K of as-made silica, APTES20, APTES40 [35], and APTES10 (Figure 2) are of type IV(a), according to the IUPAC classification [39]. The as-made silica has a BET surface area of 584 m^2/g and a BJH pore volume of 0.89 cm^3/g (Table 1), which make it an ideal support for grafting with APTES. The amount of adsorbed N_2 and the pore volume in functionalized samples (APTES10/20/40) decreased with the increase in the APTES concentrations used.

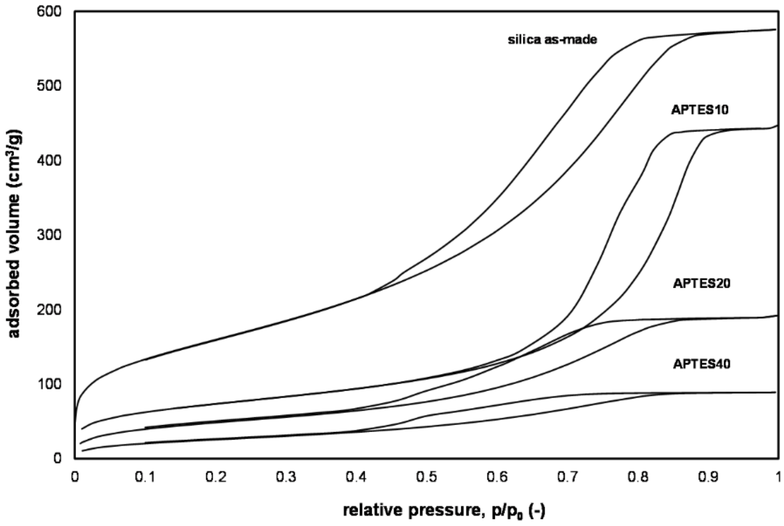

Figure 2. N_2 adsorption-desorption isotherms at 77 K for the as-made and APTES-grafted silicas: Data of as-made silica, APTES20, and APTES40 from reference [35].

As-made silica showed a pore size distribution from 3 to 20 nm; instead, the mesopores of the functionalized samples progressively occluded at increasing concentrations of the APTES solution [35].

The XRD diagram and the TGA analysis, shown in Figures 3 and 4, respectively, confirm this observation. APTES10 and APTES20 XRD spectra show a low angle peak due to the mesoscopic order of the silica support enhanced by the presence of the organosilica in the pores that increases the contrast with the amorphous silica (hump at angle 23 2θ). When APTES is absent or too concentrated, this effect is lost, and no peak at a low angle is found.

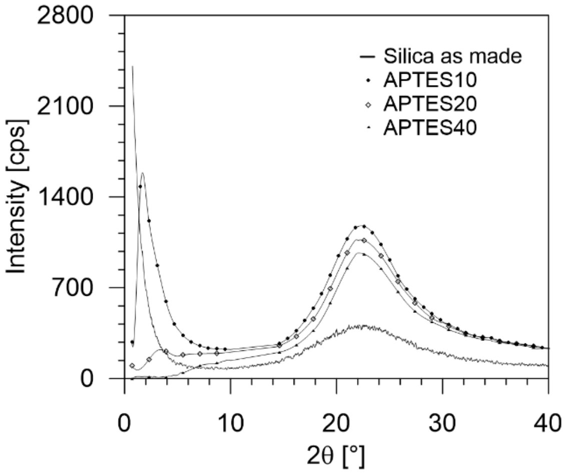

Figure 3. XRD spectra of the as-made and APTES-grafted silicas.

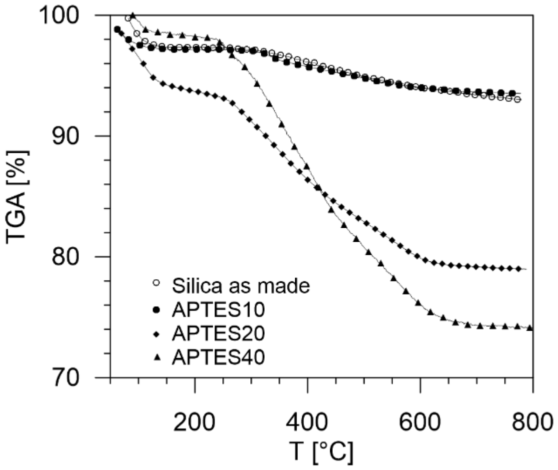

Figure 4. TG analysis of the as-made and APTES-grafted silicas before the adsorption tests data of as-made silica, APTES20, and APTES40 from reference [35].

As-made silica underwent a limited mass loss up to 150 °C, attributed to the desorption of water. A similar pattern was observed for APTES10. It seems the APTES molecules are directly linked to the surface silica and, for this reason, stable up to 750 °C. On the contrary, APTES20 and APTES40 exhibited the main mass loss between ca 300 and 600 °C, due to the degradation of the organic moieties not interacting with the silica surface. From these data, it was possible to determine the amount of the organic moieties present in each sample, as reported in Table 2.

Table 2. Content of APTES in the adsorbent particles.

Adsorbent	*T* (°C)	nAPTES (mmol APTES/mol Silica)
APTES10	330–400	16.6
APTES20	280–420	55.5
APTES40	360–680	89.7

SEM micrographs of the APTES10 sample are also reported. APTES10 (Figure 5a) particles are similar to the as-made analog (micrograph not reported), so not influenced by the grafting procedure. Higher magnification of the particles (Figure 5b) highlights the presence of rare, small aggregates of aminated organosilica formed by hydrolysis and condensation of APTES.

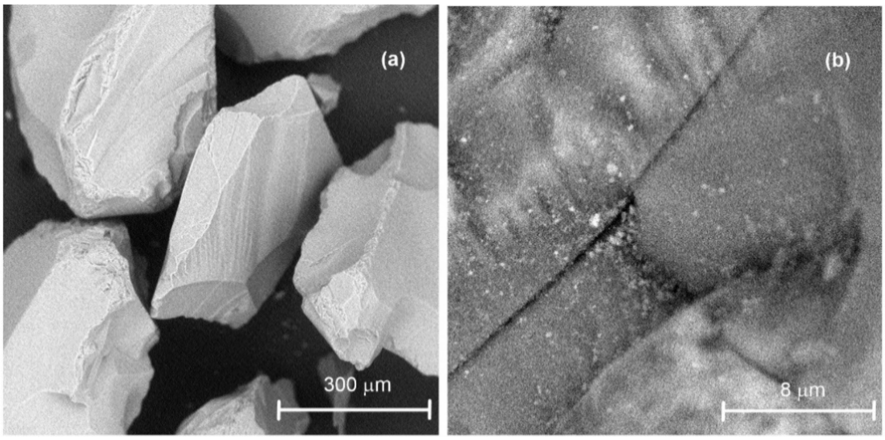

Figure 5. Micrographs of APTES10 sample: (**a**) Magnification 290×; (**b**) Magnification 10,000×.

A fluid-dynamic characterization was conducted both in a conventional layout, i.e., without packing, and in a confined one, with a packing of glass beads (d_p = 11 mm and ρ_p = 2480 kg/m^3). The fluidization of the fine sorbent into the interstitial voidage (equal to ε_p = 0.44) created by the packing avoids the occurrence of a bubbling regime and improves the efficiency of mass and heat exchange [37,40]. Since experimental investigation aimed to quantify how the suppression of the bubble phase improves the performance of the adsorption process, both types of experiments were carried out and compared. All tests were performed at ambient temperature and pressure.

In a typical experiment of conventional fluidization, an amount of sorbent was loaded in the column and, after a complete fluidization-defluidization cycle, its height was measured to determine the bed voidage. Gas velocity was gradually increased, and the corresponding pressure drop was measured, resulting in the typical fluidization diagrams shown in Figure 6. The characteristic fluidization velocities and corresponding voidage values were collected in Table 3.

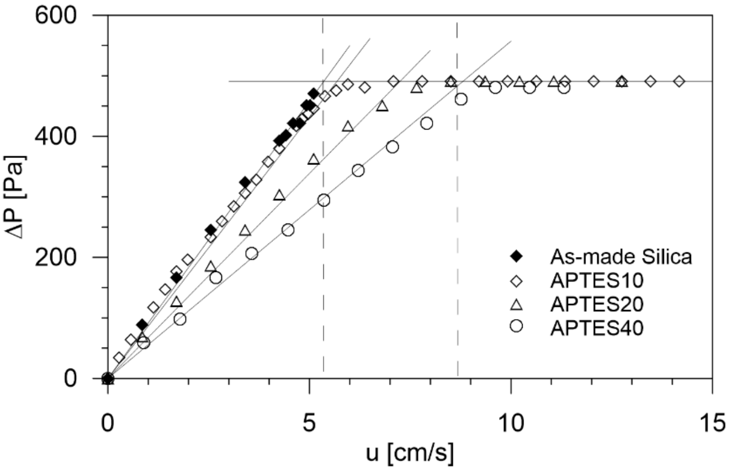

Figure 6. Diagram of the conventional fluidization tests on all samples investigated.

Table 3. Conventional fluidization properties of the adsorbent particles.

Adsorbent	ε (-)	u_{mf} (10^{-2} m/s)
As-made Silica	0.430	5.15
APTES10	0.473	5.52
APTES20	0.483	7.14
APTES40	0.490	8.63

Different values of u_{mf} were obtained for the samples, from a minimum of 5.15 to a maximum of 8.63 cm/s, due to the change of particle density after functionalization and also to the different values of bed voidage. Probably, the effect of impregnation also changed the properties of the external surface, modifying the interparticle forces that rule the bulk voidage.

Concerning the confined fluidization experiments, as indicated in a previous study [35], preliminarily, a packing of coarse spheres with a height of 450 mm was poured onto the column. Then, 100 g of the finer sorbent was loaded in the column and, after a complete fluidization-defluidization cycle, its height was measured. The bed voidage in the packed-fluidized bed and the fraction of volume available to the gas flow were calculated (Table 4) according to the definitions reported in the previous article [35].

Table 4. Confined fluidization properties of the adsorbent particles.

Adsorbent	u_{mfc} **(10^{-2} m/s)**	ε **(-)**	$\varepsilon_{fc} = \varepsilon/\varepsilon_p$ **(-)**	u_0 **(10^{-2} m/s)**	n **(-)**	**Ref.**
As-made Silica	3.1	0.236	0.537	189	5.4	[35]
APTES10	3.2	0.230	0.535	208	5.8	This work
APTES20	4.5	0.237	0.539	187	4.9	[35]
APTES40	5.6	0.233	0.530	204	4.3	[35]

The dependence of particle density by functionalization produced different values of u_{mfc} also in the confined system tests, as shown in Figure 7. The homogeneous expansion trends of u/ε_p versus ε_{fc} were also determined (figure here not reported). Among the characteristic parameters (see Table 4), ε_{fc} and u_0 appear more constant, while the exponent n decreases for higher concentrations of APTES [35].

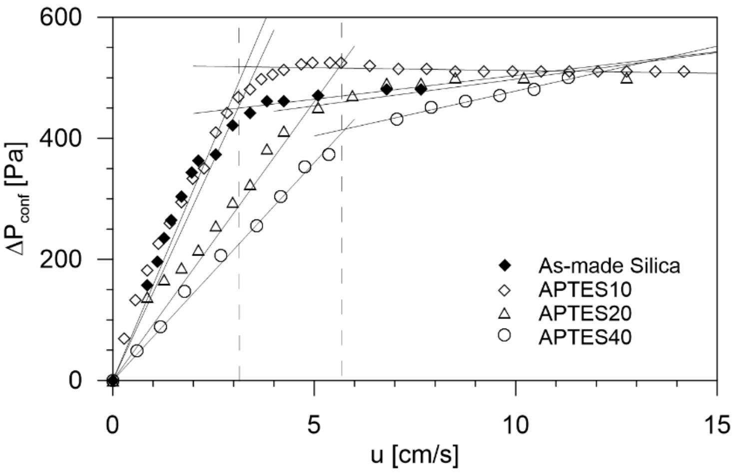

Figure 7. Diagram of confined fluidization tests on all samples investigated: data of as-made silica, APTES20, and APTES40 from reference [35].

The observed regular homogeneous expansion was described by a modified form of the Richardson and Zaki's equation [41], in which the exponent n and u_0 were calculated according to a method reported in a previous work [42].

The effect of fluidization conditions in conventional and confined layouts during adsorption tests was explored, setting, first, the optimal superficial velocity of the gaseous mixture (CO_2/air) fed to the column, taking into account the previously performed fluid-dynamic characterization.

For each of the two contact modes, various CO_2 concentrations of the incoming stream were explored for the same amount of sorbent.

The breakthrough curves were obtained, measuring the CO_2 concentration at the exit of the bed at prefixed times. In addition, the temperature was measured using a thermocouple inside the bed.

Once fixed the surface velocity, it was possible, knowing the column section, to calculate the flow rate of the inlet gaseous mixture:

$$Q_{mix} = u \cdot A \tag{1}$$

From the total volumetric flow rate, it was possible to calculate the air and the CO_2 flow rates based on the volumetric concentration of CO_2 fixed in the various tests:

$$Q_{CO_2} = Q_{mix} x_{CO_2} \tag{2}$$

$$Q_{air} = Q_{mix}\left(1 - x_{CO_2}\right) \tag{3}$$

The contact time for this continuous process is defined as:

$$t_c = \frac{V_{open}}{Q_{mix}} \tag{4}$$

where

$$V_{open} = \begin{cases} AH_{f,mf} - \frac{m_f}{\rho_f} \; for\ conventional\ fluidization \\ AH_{fc}\epsilon_p - \frac{m_f}{\rho_f} \; for\ confined\ fluidization \end{cases} \tag{5}$$

and Q_{mix}, the inlet flow rate of the mixture, is given by:

$$Q_{mix} = A\,u = Q_{air} + Q_{CO_2} \tag{6}$$

A differential balance in time was obtained on the column:

$$\frac{dm}{dt} = \frac{\pi_{in}\, Q_{CO2}^{in}\, MW}{RT_{in}} - \frac{\pi_{out}\, Q_{CO2}^{out}\, MW}{RT_{out}} \tag{7}$$

where

$\frac{dm}{dt}$ represented the amount of CO_2 that accumulates on solid sorbent, T_{in}, T_{out}, π_{in}, π_{out} were respectively the inlet and outlet stream temperature and pressure of the column.

The pressure and temperature of the gas stream can be assumed constant. The volumetric flow rates change due to adsorption. Knowing the composition of CO_2 entering and leaving the column, the volumetric flow rates can be calculated as a function of the total gas flow rate:

$$Q_{CO2}^{in} = Q_{mix} x_{CO2}^{in} \tag{8}$$

$$Q_{CO2}^{out} = Q_{mix} x_{CO2}^{out} \tag{9}$$

$$\frac{dm}{dt} = MW\frac{\pi}{RT}\left(Q_{mix}x_{CO2}^{in} - Q_{mix}x_{CO2}^{out}\right) \tag{10}$$

It was possible to rearrange the balance equation in:

$$\frac{dm}{dt} = MW\frac{\pi}{RT}\, Q_{mix}x_{CO2}^{in}\left(1 - \frac{x_{CO2}^{out}}{x_{CO2}^{in}}\right) \tag{11}$$

Finally, the integration provides the amount of CO_2 adsorbed as a function of the operating time of the process:

$$m = MW\frac{\pi}{RT}\, Q_{mix}x_{CO2}^{in}\int_0^{t_s}\left(1 - \frac{x_{CO2}^{out}}{x_{CO2}^{in}}\right)dt \tag{12}$$

For each experiment, the gas velocity and the inlet concentration of CO_2 were set. Considering the minimum fluidization velocity in a conventional environment, previously obtained for functionalized silica, two values were explored: $0.8u_{mf}$ for the fixed bed and $1.20u_{mf}$ for the bubbling bed. It is worth recalling that in a confined layout, sorbent was in the homogeneous expansion condition at these values of gas velocity.

3.2. Effect of the Concentration of APTES on Amino-Functionalized Silica

Before exploring the effect of the layout, a preliminary adsorption campaign was devoted to the analysis of the performance of the sorbent versus the concentration of APTES used for its functionalization. To this aim, a mixture with 12% of CO_2 was fed to a bed in the confined layout at u = 4.4 cm/s for APTES10, like it was made at u = 5.6 cm/s for APTES20 and at u = 6.9 cm/s for APTES40, in a previous investigation [35]. The intent of the test in confined fluidization was to analyze the adsorption process in the more favorable regime of homogeneous expansion of the adsorbent.

The comparison of the amount of CO_2 adsorbed, m, and the bed fraction used, W, (Table 5) between silica and functionalized samples for a stream of 12% CO_2 shows as the presence of APTES had definitely improved the adsorption capacity.

Table 5. The adsorption performance of as-made silica and amino-functionalized samples in terms of two characteristic parameters: inlet gas at 12% CO_2; confined layout.

At x_{CO2} = 12%	As-Made Silica	APTES10	APTES20	APTES40
m (mg/g)	6.20	22.2	29.9	32.5
W (%)	68.7	49.5	78.0	20.5

The adsorption capacity, which was practically unchanged, passing from APTES40 to APTES20, decreased significantly for the APTES10 sample. Probably the 10% solution did not sufficiently modify the active sites able of capturing CO_2. Although the amount of adsorbed CO_2 was slightly higher for APTES40, this sample used a significantly lower bed fraction, indicating slow saturation kinetics and consequently insufficient use of the sorbent up to the breakpoint.

In fact, the breakthrough curves at the fixed concentration of CO_2 (12%) in Figure 8 confirmed that: for a continuous process, the optimum was obtained with the APTES20 sample. The breakthrough curve had a higher time of breakpoint, indicating that this sorbent could capture CO_2 for a longer time during an industrial process. The saturation time was lower than the APTES40 sample time, suggesting that faster adsorption kinetics correlates with greater active surface availability.

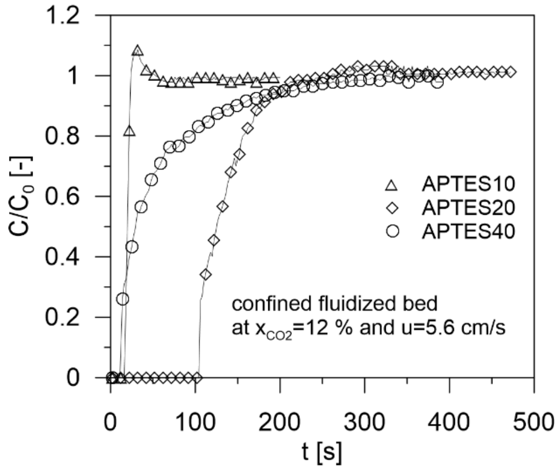

Figure 8. Breakthrough curves at a fixed concentration of CO_2 (12%) for functionalized silica.

For these reasons, dynamic adsorption tests were completed at several compositions of the inlet mixture only on the sample APTES20.

3.3. Effect of the CO_2 Concentration of Inlet Gas

For the adsorption tests on APTES20, seven concentrations (5%, 8%, 10%, 12%, 15%, 18%, 20%) for both velocities were explored.

In Figures 9 and 10, two breakthrough curves and corresponding temperatures are compared for the velocity 5.6 cm/s in which sorbent was in fixed bed in conventional fluidization or moderately expanded in confined fluidization. The same comparison is reported in Figures 11 and 12 for the velocity 8.6 cm/s that was sufficient to determine the bubbling regime in the conventional fluidization in contrast with the extended homogeneous expansion of the sorbent in the confined bed.

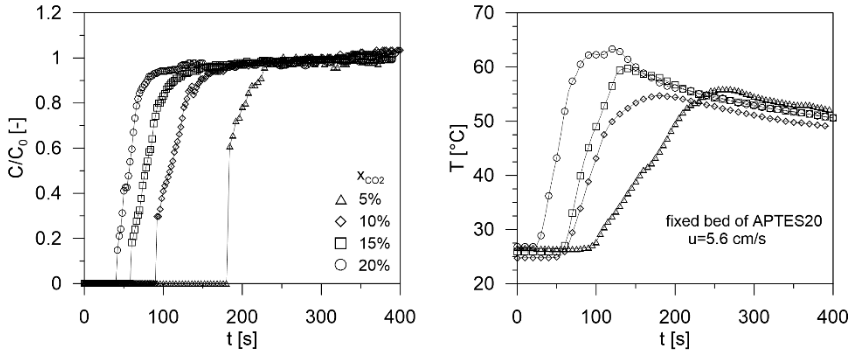

Figure 9. Breakthrough curves and corresponding temperature at different CO_2 concentrations for APTES20 in conventional fixed bed at u = 5.6 cm/s.

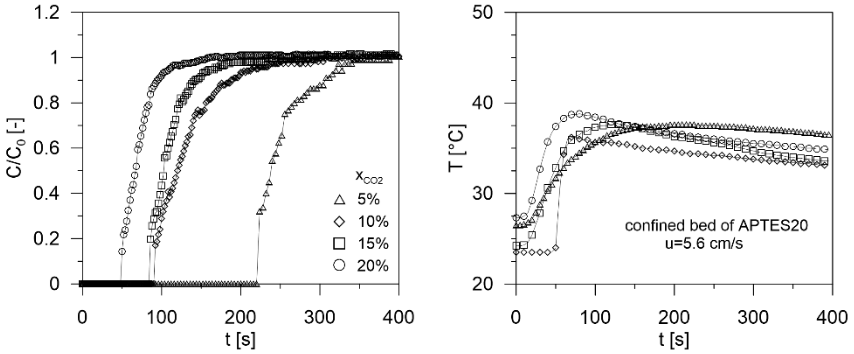

Figure 10. Breakthrough curves and corresponding temperature at different CO_2 concentrations for APTES20 in confined expanded bed at u = 5.6 cm/s.

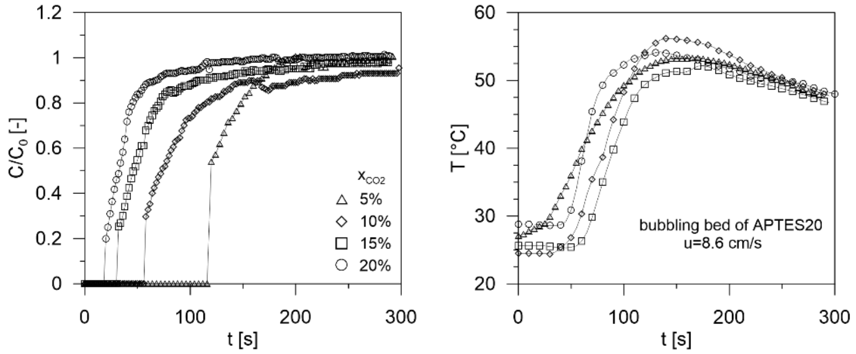

Figure 11. Breakthrough curves and corresponding temperature at different CO_2 concentrations for APTES20 in conventional bubbling bed at u = 8.6 cm/s.

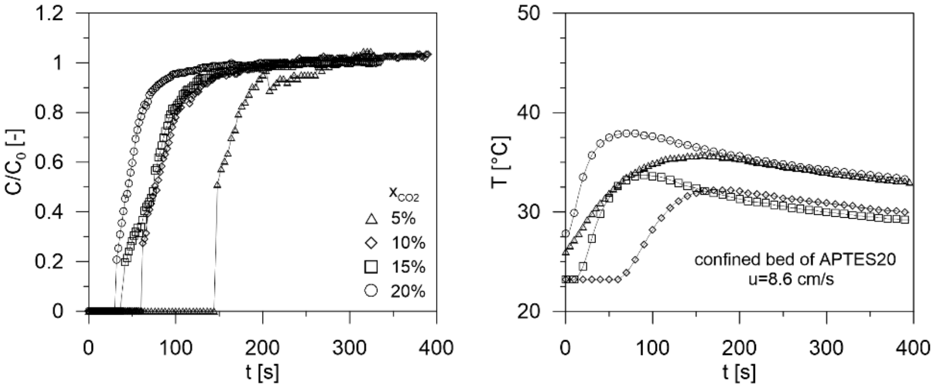

Figure 12. Breakthrough curves and corresponding temperature at different CO_2 concentrations for APTES20 in confined expanded bed at u = 8.6 cm/s.

Regardless of the velocity value, the increased inlet concentration of CO_2 in the gas mixture reduced the times of the adsorption curves and increased the maximum temperature determined in the bed. In the confined layout, times were longer because of the higher contact times, while, on the contrary, a lower level of thermal effects was detected.

The occurring of the bubbling regime had already reduced the temperature in the conventional layout (see Figure 11), while only the homogeneous fluidization of the particles in the confined bed allows controlling the increase in the temperature into a range of at most 10 °C (see Figures 10 and 12).

3.4. *Effect of the Velocity of the Inlet Gas*

Figures 13 and 14 showing the curves obtained for the adsorption of the 15% CO_2 gas mixture, are compared at different values of velocity and at the same layout. Even though the increased velocity reduces the contact times and the breakthrough time, the bubbling regime showed better control of the temperature, lower than the 59% respect to that maximum value reached the fixed bed (ca. 50 °C) (see Figure 13). Figure 14 shows the similar effect of the velocity in the confined bed: also in this case, at higher velocity corresponds a lower characteristic time of adsorption; moreover, a reduction in temperature of 55% was detected, that in this case, reached a maximum value significantly lower of 34 °C.

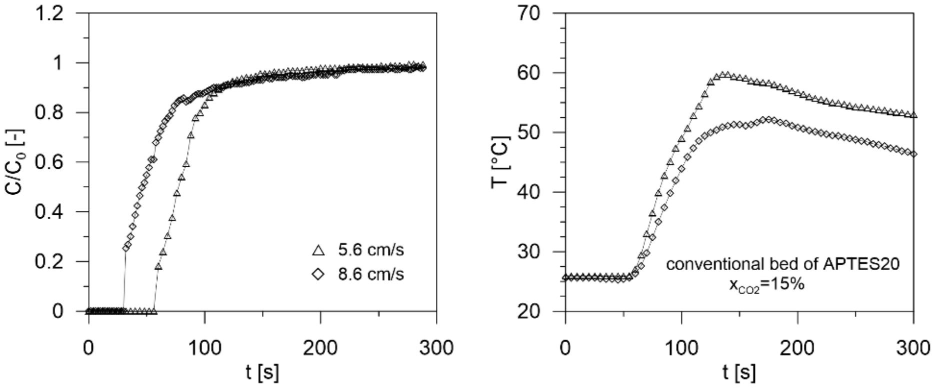

Figure 13. Effect of gas velocity on the breakthrough curves for APTES20 in conventional bed with 15% CO_2.

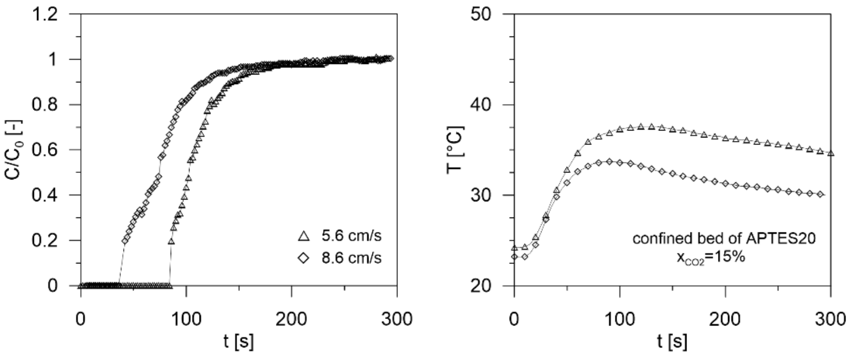

Figure 14. Effect of gas velocity on the breakthrough curves for APTES20 in confined expanded bed with 15% CO_2.

3.5. Effect of the Layout of the Gas-Adsorbent Contact

To evaluate the effect of the layout on gas-solid contact, in Figures 15 and 16, the breakthrough curves were reported at the same velocity value and 15% of CO_2 as inlet gas concentration. The breakthrough curves in the confined mode were shifted toward the right with a relative increase in the breakpoint times and with a remarkable reduction in the temperature in the bed. The breakthrough time appears higher of 45% than that obtained in conventional fixed bed (see Figure 15) and of 10% than that of bubbling bed (see Figure 16). Noteworthy is the favorable control of the thermal effects: the confined expanded bed showed a maximum temperature of 38 °C with respect to the temperature of 60 °C reached in the fixed bed. Finally, the T_{max} was 52 °C for the bubbling bed and 34 °C for the confined layout.

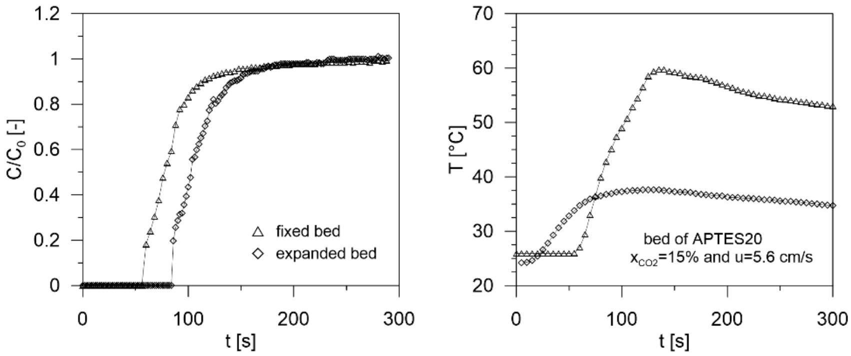

Figure 15. The breakthrough curves of APTES20 at a fixed velocity (5.6 cm/s) and concentration (15% CO_2) for both contact modes.

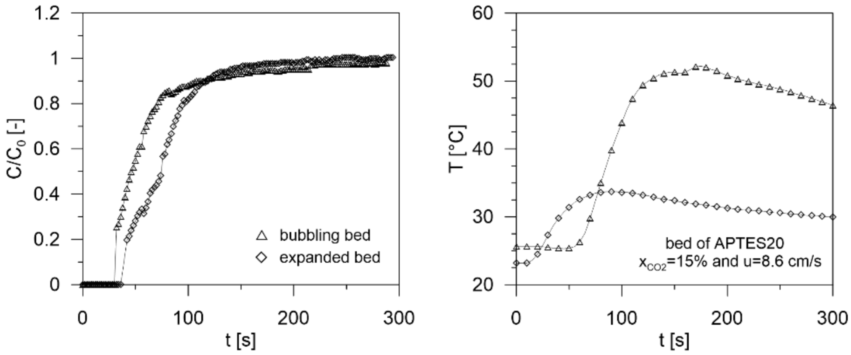

Figure 16. The breakthrough curves of APTES20 at a fixed velocity (8.6 cm/s) and concentration (15% CO_2) for both contact modes.

The beneficial effect of the contact mode in a confined environment (Figures 17–20) was evaluated by the analysis of the characteristic parameters (summarized in Table 6) at different CO_2 concentrations.

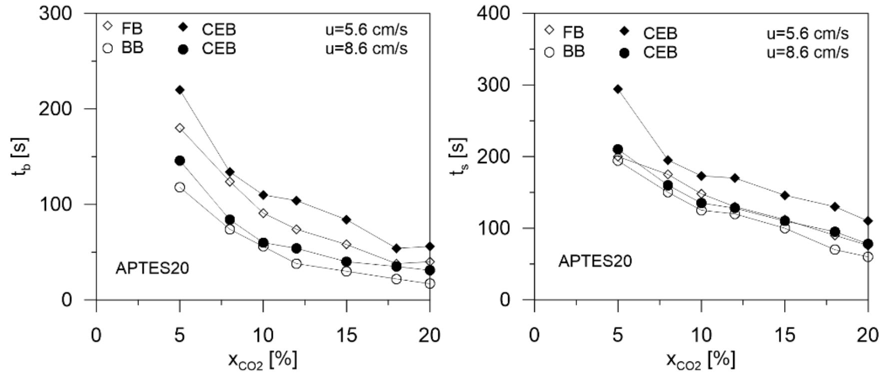

Figure 17. Breakpoint and saturation times at increasing CO_2 concentrations for APTES20 at different contact modes and at two velocities.

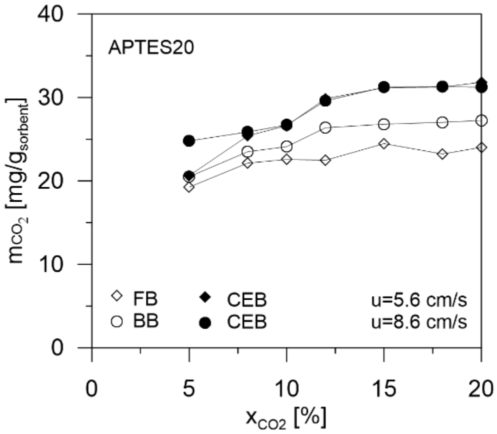

Figure 18. Mass of CO_2 adsorbed on adsorbent at increasing CO_2 concentrations for APTES20 at different contact modes and at two velocities.

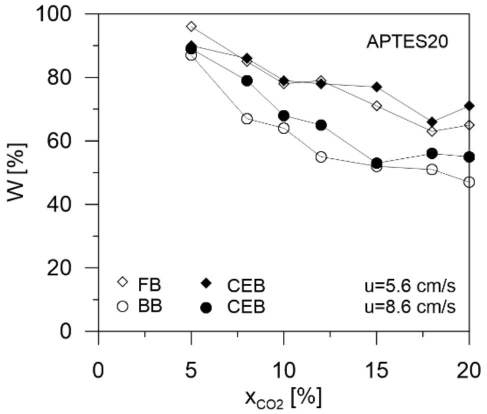

Figure 19. Fraction of bed used at increasing CO_2 concentrations for APTES20 at different contact modes and at two velocities.

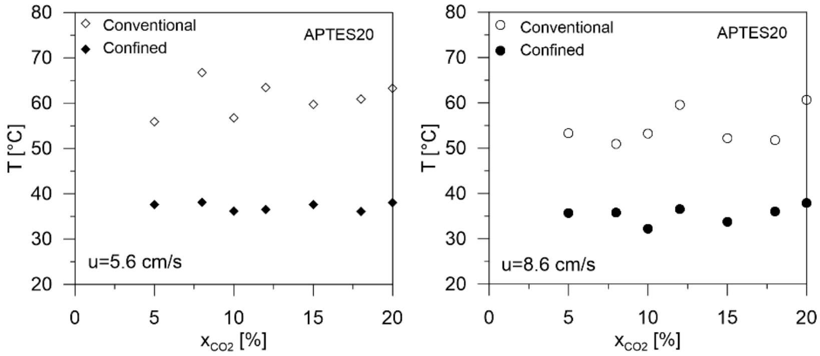

Figure 20. Temperature trend as a function of CO_2 concentration for APTES20 at different contact modes and at two velocities.

Table 6. Characteristic parameters of the adsorption tests on APTES20 for different values of gas velocity, for different layouts, and at varying inlet gas concentrations of CO_2. (* FB: fixed bed; BB: bubbling bed; CEB: confined expanded bed).

%CO_2	u (cm/s)	Contact Mode	t_c (s)	t_b (s)	t_s (s)	m_{CO2} (mg/g)	W (%)	T_{max} (°C)
5	5.6	FB *	0.69	180	200	19.26	96	55.9
		CEB *	0.68	220	294	20.64	90	37.6
	8.6	BB *	0.46	118	194	20.51	87	53.3
		CEB	0.57	146	210	24.80	89	35.7
8	5.6	FB	0.59	124	175	22.14	85	66.7
		CEB	0.69	134	195	25.40	86	38.1
	8.6	BB	0.39	74	150	23.50	67	50.9
		CEB	0.56	84	160	25.87	79	35.8
10	5.6	FB	0.68	91	148	22.57	78	56.7
		CEB	0.71	110	173	26.63	79	36.2
	8.6	BB	0.42	56	125	24.11	64	53.2
		CEB	0.55	60	135	26.70	68	32.2
12	5.6	FB	0.60	74	130	22.48	79	63.4
		CEB	0.68	104	170	29.86	78	36.5
	8.6	BB	0.40	38	120	26.38	55	59.6
		CEB	0.57	54	128	29.60	65	36.5
15	5.6	FB	0.64	58	112	24.47	71	59.7
		CEB	0.68	84	146	31.18	77	37.6
	8.6	BB	0.43	30	100	26.80	52	52.2
		CEB	0.55	40	110	31.24	53	33.7
18	5.6	FB	0.69	38	90	23.23	63	60.9
		CEB	0.70	54	130	31.25	66	36.1
	8.6	BB	0.46	22	70	27.02	51	51.8
		CEB	0.54	35	95	31.30	56	36.0
20	5.6	FB	0.70	40	76	24.03	65	63.3
		CEB	0.69	56	110	31.83	71	38.0
	8.6	BB	0.46	17	60	27.25	47	60.7
		CEB	0.56	31	78	31.22	55	37.9

All the parameters analyzed had indicated that a substantial improvement of the adsorption performance in the confined layout was obtained.

Even if the contact times decreased with increasing velocity, comparing the conventional and the confined layout at the same velocity, they were higher by about 40%.

The improved contact performance was then confirmed by the characteristic breakpoint and saturation times, as illustrated in Figure 17.

Considering the decreasing trend of the characteristic times as the inlet CO_2 concentration in the gas mixture increased, a quadratic dependence was observed for the breakthrough time and an almost linear dependence for the saturation time. In both cases, in a confined environment, the values of the characteristic times were slightly higher than in the conventional mode at both velocities.

The amount of CO_2 adsorbed, shown in Figure 18, increased with the inlet CO_2 concentration to reach a plateau, regardless of velocities and modes of contact. Moreover, in the confined layout, the constant value of ca. 31 mg/g of the adsorbent was the maximum reached regardless of the level of the expansion. It was evident the difference existing between the quantities adsorbed in the two contact modes, especially at the lower velocity, which suggests significantly improved performance in the confined mode.

As shown in Figure 19, the fraction of bed used up to the breakpoint confirmed that a higher value, in confined mode, was also obtained.

The fraction of bed used up to the breakpoint decreased as the concentration of CO_2 increased. This trend is more evident for higher velocities. However, the difference in the confined bed was not too noticeable such as in terms of mass adsorbed.

Finally, the temperature of the bed during adsorption in the two contact modes and velocities versus the inlet CO_2 concentration in the mixture is reported in Figure 20.

These results are explained considering that CO_2 adsorption is an exothermic process. Then, any temperature increase was not favorable to the adsorption performance of the bed. Of course, the fixed bed had lower performance, while bubbling or expanded beds were more able to reduce the variation of the operating temperature. Each contact mode had a typical thermal level, higher for the conventional bed (between 50 and 60 °C) and lower for the confined bed (between 30 and 40 °C). The temperatures were not particularly sensitive to velocity and concentration variations.

Table 7 summarizes the CO_2 adsorption values for mesoporous samples, as reported in previous works, modified using several amine agents. Data presented in our work are comparable and quite promising, considering that they are obtained using a CO_2/air mixture.

Table 7. Adsorption capacity of amine-modified silica from literature.

Supporting Porous Material	Amine Type	Gas Mixture	CO_2 Adsorption (mg/g)	Ref.
SBA-15	EDA	CO_2/N_2	20	[22]
SBA-15	PEHA	CO_2/N_2	21.7	[32]
Mesoporous Silica	APTES	CO_2/N_2	21.6	[20]
Mesoporous Silica	APTES	CO_2/air	31.8	This work
SBA-15	PEI	CO_2/N_2	39.5	[43]
Mesoporous Silica	APTES	CO_2/N_2	40	[36]

4. Conclusions

In this study, an experimental campaign of CO_2 adsorption tests on APTES-grafted mesoporous silica particles was carried out. Three different APTES concentrations in the grafting solution allowed obtaining sorbents with different abilities for the CO_2 capture. Two layouts of gas-sorbent contact were explored: in conventional mode, adsorption was carried at fixed bed condition and bubbling regime; in the confined-fluidized bed, two different conditions of homogeneous expansion were obtained for two values of gas velocity.

The mesoporous silica particles have proved to be highly valid supports for efficient dispersion of the amine moieties on the active surface by grafting with APTES. Among the amino-functionalized sorbents, APTES20 exhibited the highest potentiality as sorbent in a continuous process of CO_2 capture from flue gas streams. Such ability was measured in terms of high CO_2 adsorption capacity and more efficient use of the bed of the sorbent, in particular in the confined-fluidized bed. The enhanced performance of the confined layout compared to the conventional mode of fluidization was verified for all the ranges of the inlet CO_2 concentration of the gas mixture. This is especially due to the more favorable control of the thermal effects during the adsorption cycle, which can be optimized by setting the operative gas velocity. An optimum superficial gas velocity of 5.6 cm/s was obtained for the CO_2 adsorption process on APTES20 in a confined-fluidized layout.

Finally, this amino-based sorbent exhibited high thermal stability and a relatively low temperature of regeneration (about 120 °C).

The fluid-dynamic and thermal characterization of adsorption/regeneration of the sorbent together with the easy and green grafting procedure of the mesoporous silica indicates this approach to the CO_2 capture as an attractive and competitive process to be applied in the industrial contest.

Author Contributions: Conceptualization, R.G. and M.T.; methodology, R.G.; software, M.G., G.G. and M.T.; validation, R.G., F.T., M.G. and G.G.; formal analysis, R.G. and F.T.; investigation, G.L. and M.T.; resources, R.G. and F.T.; data curation, R.G. and F.T.; writing—original draft preparation, R.G., F.T. and M.T.; writing—review and editing, R.G., F.T., M.T. and G.G.; visualization, R.G.; supervision, R.G. and F.T.; project administration, F.T.; funding acquisition, F.T. All authors have read and agreed to the published version of the manuscript.

Funding: This research was funded by MIUR, PRIN 2017 "Nanostructured Porous Ceramics for Environmental and Energy Applications", grant number 2017PMR932_005.

Institutional Review Board Statement: Not applicable.

Informed Consent Statement: Not applicable.

Acknowledgments: The support of the PON SILA project (code: PONa3_00341 funded by Italian ministries MIUR and MISE) with the availability of the Sympatec-Qicpic and laser diffractometer Sympatec Helos measurement devices is gratefully acknowledged.

Conflicts of Interest: The authors declare no conflict of interest.

Notation

A	column section, cm^2
C/C_0	dimensionless CO_2 fraction in the effluent gas, -
D	column diameter, cm
d_p	diameter of glass beads, mm
H_{fc}	sorbent height in confined bed, cm
m_{CO2}	mass of CO_2 adsorbed per unit mass of sorbent, $mgCO_2/g_{\text{ sorbent}}$
m	mass of sorbent bed, g
n	expansion index, -
π_{in}	pressure of inlet stream, atm
π_{out}	pressure of outlet stream, atm
Q_{air}	volumetric flow rate of air, cm^3/s
Q_{CO2}	volumetric flow rate of CO_2, cm^3/s
Q_{mix}	volumetric flow rate of gas mixture, cm^3/s
R	gas constant, atm/mol K
t	time, s
t_b	breakthrough time in the confined bed, s
t_c	contact time in the confined bed, s
t_s	saturation time in the confined bed, s
T	temperature in the middle of the confined-fluidized bed, °C
T_{in}	temperature of inlet stream, °C
T_{max}	maximum temperature in the middle of the confined-fluidized bed, °C
T_{out}	temperature of outlet stream, °C
u	superficial gas velocity, cm/s
u_{mfc}	minimum fluidization velocity of the confined bed, cm/s
u_0	maximum expansion velocity of the confined bed, cm/s
V	geometrical volume of the solid, cm^3

V_{open}	volume available to gas, cm^3
Wf	fraction of bed utilized at breakpoint, %
x_{CO2}	CO_2 fraction in the inlet gas, % vol
Greek Symbols	
ΔP_{conf}	pressure drop in the confined system, Pa
ε	voidage in the packed-fluidized bed, -
ε_{fc}	voidage of the equivalent conventional bed, -
ε_p	voidage of the packed bed, -
ρ	particle density of solid, kg/m^3
ρ_p	particle density of glass beads, kg/m^3

References

1. IEA. *CCUS in Clean Energy Transitions*; IEA: Paris, France, 2020; Available online: https://www.iea.org/reports/ccus-in-clean-energy-transitions (accessed on 10 January 2022).
2. Choi, S.; Drese, J.H.; Jones, C.W. Adsorbent Materials for Carbon Dioxide Capture from Large Anthropogenic Point Sources. *Chem. Sus. Chem.* **2009**, *2*, 796–854. [CrossRef] [PubMed]
3. Ho, M.T.; Allinson, G.W.; Wiley, D.E. Reducing the Cost of CO_2 Capture from Flue Gases Using Pressure Swing Adsorption. *Ind. Eng. Chem. Res.* **2008**, *47*, 4883–4890. [CrossRef]
4. Sayari, A.; Belmabkhout, Y.; Serna-Guerrero, R. Flue Gas treatment via CO_2 adsorption. *Chem. Eng. J.* **2011**, *171*, 760–774. [CrossRef]
5. Rezaei, F.; Sakwa-Novak, M.A.; Bali, S.; Duncanson, D.M.; Jones, C.W. Shaping amine-based solid CO_2 adsorbents: Effects of pelletization pressure on the physical and chemical properties. *Microporous Mesoporous Mater.* **2015**, *204*, 34–42. [CrossRef]
6. Santiago, R.G.; Siqueira, R.M.; Alves, C.A.; Vilarrasa-García, E.; Maia, D.A.S.; Bastos-Neto, M.; Azevedo, D.C.S.D. Evaluation of the thermal regeneration of an amine-grafted mesoporous silica used for CO_2/N_2 separation. *Adsorption* **2020**, *26*, 203–215. [CrossRef]
7. Wang, Q.; Luo, J.; Zhong, Z.; Borgna, A. CO_2 capture by solid adsorbents and their applications: Current status and new trends. *Energy Environ. Sci.* **2011**, *4*, 42–55. [CrossRef]
8. Plaza, M.G.; Pevida, C.; Arias, B.; Casal, M.D.; Martın, C.F.; Fermoso, J.; Rubiera, F.; Pis, J.J. Different approaches for the development of low-cost CO_2 adsorbents. *J. Environ. Eng.* **2009**, *135*, 426–432. [CrossRef]
9. Mercedes Maroto-Valer, M.; Tang, Z.; Zhang, Y. CO_2 capture by activated and impregnated anthracites. *Fuel Process. Technol.* **2005**, *86*, 1487–1502. [CrossRef]
10. Zhao, C.; Chen, X.; Zhao, C. Study on CO_2 capture using dry potassium-based sorbents through orthogonal test method. *Int. J. Greenh. Gas Control* **2010**, *4*, 655–658. [CrossRef]
11. Younas, M.; Sohail, M.; Leong, M.J.B.L.K.; Sumathi, S. Feasibility of CO_2 adsorption by solid adsorbents: A review on low-temperature systems. *Int. J. Environ. Sci. Technol.* **2016**, *13*, 1839–1860. [CrossRef]
12. Poshusta, J.C.; Tuan, V.A.; Pape, E.A.; Noble, R.D.; Falconer, J.L. Separation of light gas mixtures using SAPO-34 membranes. *AIChE J.* **2004**, *46*, 779–789. [CrossRef]
13. Samanta, A.; Zhao, A.; Shimizu, G.K.H.; Sarkar, P.; Gupta, R. Postcombustion CO_2 capture using solid sorbents. *Ind. Eng. Chem. Res.* **2011**, *51*, 1438–1463. [CrossRef]
14. Ho, T.H.; Howes, T.; Bhandari, B.R. Encapsulation of gases in powder solid matrices and their applications: A review. *Powder Technol.* **2014**, *259*, 87–108. [CrossRef]
15. Yoon, J.H.; Heo, N.H. A study on hydrogen encapsulation in CS2.5-zeolite A. *J. Phys. Chem.* **1992**, *96*, 4997–5000. [CrossRef]
16. Le Thi, M.U.; Lee, S.-Y.; Park, S.-J. Preparation and characterization of PEI-loaded MCM-41 for CO_2 capture. *Int. J. Hydrogen Energy* **2014**, *39*, 12340–12346. [CrossRef]
17. Kim, S.; Ida, J.; Guliants, V.V.; Lin, Y.S. Tailoring pore properties of MCM-48 silica for selective adsorption of CO_2. *J. Phys. Chem. B* **2005**, *109*, 6287–6293. [CrossRef] [PubMed]
18. Sanz, R.; Calleja, G.; Arencibia, A.; Sanz-Pérez, E.S. Amino functionalized mesostructured SBA-15 silica for CO_2 capture: Exploring the relation between the adsorption capacity and the distribution of amino groups by TEM. *Microporous Mesoporous Mater.* **2012**, *158*, 309–317. [CrossRef]
19. Yan, X.; Zhang, L.; Zhang, Y.; Yang, G.; Yan, Z. Amine-modified SBA-15: Effect of pore structure on the performance for CO_2 capture. *Ind. Eng. Chem. Res.* **2011**, *50*, 3220–3226. [CrossRef]
20. Leal, O.; Bolívar, C.; Ovalles, C.; García, J.J.; Espidel, Y. Reversible adsorption of carbon dioxide on amine surface-bonded silica gel. *Inorg. Chim. Acta* **1995**, *240*, 183–189. [CrossRef]
21. Zhao, A.; Samanta, A.; Sarkar, P.; Gupta, R. Carbon dioxide adsorption on amineimpregnated mesoporous SBA-15 sorbents: Experimental and kinetics study. *Ind. Eng. Chem. Res.* **2013**, *52*, 6480–6491. [CrossRef]
22. Zheng, F.; Tran, D.N.; Busche, B.J.; Fryxell, G.E.; Addleman, R.S.; Zemanian, T.S.; Aardahl, C.L. Ethylenediamine-modified SBA-15 as regenerable CO_2 sorbent. *Ind. Eng. Chem. Res.* **2005**, *44*, 3099–3105. [CrossRef]
23. Zhou, L.; Fan, J.; Cui, G.; Shang, X.; Tang, Q.; Wang, J.; Fan, M. Highly efficient and reversible CO_2 adsorption by amine- grafted platelet SBA-15 with expanded pore diameter and short mesochannels. *Green Chem.* **2014**, *16*, 4009–4016. [CrossRef]

24. Sanz-Pérez, E.S.; Arencibia, A.; Sanz, R.; Calleja, G. New developments on carbon dioxide capture using amine-impregnated silicas. *Adsorption* **2016**, *22*, 609–619. [CrossRef]
25. Jung, H.; Lee, C.H.; Jeon, S.; Jo, D.H.; Huh, J.; Kim, S.H. Effect of amine double-functionalization on CO_2 adsorption behaviors of silica gel-supported adsorbents. *Adsorption* **2016**, *22*, 1137–1146. [CrossRef]
26. Yue, M.B.; Chun, Y.; Cao, Y.; Dong, X.; Zhu, X.J.H. CO_2 capture by as-prepared SBA-15 with an occluded organic template. *Adv. Funct. Mater.* **2006**, *16*, 1717–1722. [CrossRef]
27. Yue, M.B.; Sun, L.B.; Cao, Y.; Wang, Z.J.; Wang, Y.; Yu, Q.; Zhu, J.H. Promoting the CO_2 adsorption in the amine-containing SBA-15 by hydroxyl group. *Microporous Mesoporous Mater.* **2008**, *114*, 74–81. [CrossRef]
28. Anyanwu, J.-T.; Wang, J.; Yang, R.T. Amine-Grafted Silica Gels for CO_2 Capture Including Direct Air Capture. *Ind. Eng. Chem. Res.* **2020**, *59*, 7072–7079. [CrossRef]
29. Wu, J.; Zhu, X.; Yang, F.; Ge, T.; Wang, R. Easily-synthesized and low-cost amine-functionalized silica sol-coated structured adsorbents for CO_2 capture. *Chem. Eng. J.* **2021**, *425*, 131409. [CrossRef]
30. Sanz-Pérez, E.S.; Olivares-Marín, M.; Arencibia, A.; Sanz, R.; Calleja, G.; Maroto-Valer, M.M. CO_2 adsorption performance of aminofunctionalized SBA-15 under post-combustion conditions. *Int. J. Greenh. Gas Control* **2013**, *17*, 366–375. [CrossRef]
31. Vilarrasa-García, E.; Cecilia, J.A.; Santos, S.M.L.; Cavalcante, C.L.; Jiménez-Jiménez, J.; Azevedo, D.C.S.; Rodríguez-Castellón, E. CO_2 adsorption on APTES functionalized mesocellular foams obtained from mesoporous silicas. *Microporous Mesoporous Mater.* **2014**, *187*, 125–134. [CrossRef]
32. Wei, L.; Gao, Z.; Jing, Y.; Wang, Y. Adsorption of CO_2 from simulated flue gas on pentaethylenehexamine-loaded mesoporous silica support adsorbent. *Ind. Eng. Chem. Res.* **2013**, *52*, 14965–14974. [CrossRef]
33. Lashaki, M.J.; Khiavi, S.; Sayari, A. Stability of amine-functionalized CO_2 adsorbents: A multifaceted puzzle. *Chem. Soc. Rev.* **2019**, *48*, 3320. [CrossRef] [PubMed]
34. Varghese, A.M.; Karanikolos, G.N. CO_2 capture adsorbents functionalized by amine–bearing polymers: A review. *Int. J. Greenh. Gas Control* **2020**, *96*, 103005. [CrossRef]
35. Girimonte, R.; Testa, F.; Gallo, M.; Buscieti, R.; Leone, G.; Formisani, B. Adsorption of CO_2 on Amine-Modified Silica Particles in a Confined-Fluidized Bed. *Processes* **2020**, *8*, 1531. [CrossRef]
36. Quang, D.V.; Alan Hatton, T.; Abu-Zahra, M.R.M. Thermally Stable Amine-Grafted Adsorbent Prepared by Impregnating 3-Aminopropyltriethoxysilane on Mesoporous Silica for CO_2 Capture. *Ind. Eng. Chem. Res.* **2016**, *55*, 7841–7852. [CrossRef]
37. Girimonte, R.; Formisani, B.; Testa, F. Adsorption of CO_2 on a confined fluidized bed of pelletized 13X zeolite. *Powder Technol.* **2017**, *311*, 9–17. [CrossRef]
38. Abrahamsen, A.R.; Geldart, D. Behaviour of gas-fluidized beds of fine powders, part I. Homogeneous expansion. *Powder Technol.* **1980**, *26*, 35–46. [CrossRef]
39. Thommes, M.; Kaneko, K.; Neimark, A.V.; Olivier, J.P.; Rodriguez-Reinoso, F.; Rouquerol, J.; Sing, K.S.W. Physisorption of gases, with special reference to the evaluation of surface area and pore size distribution (IUPAC Technical Report). *Pure Appl. Chem.* **2015**, *87*, 1051–1069. [CrossRef]
40. Girimonte, R.; Formisani, B.; Testa, F. CO_2 adsorption in a confined fluidized bed of zeolite pellets: Influence of operating velocity. *Particuology* **2019**, *46*, 67–74. [CrossRef]
41. Girimonte, R.; Vivacqua, V. Design criteria for homogeneous fluidization of Geldart's class B solids upward through a packed bed. *Powder Technol.* **2013**, *249*, 316–322. [CrossRef]
42. Girimonte, R.; Vivacqua, V. The expansion process of particle beds fluidized in the voids of a packing of coarse spheres. *Powder Technol.* **2011**, *213*, 63–69. [CrossRef]
43. Henao, W.; Jaramillo, L.Y.; López, D.; Romero-Sáez, M.; Buitrago-Sierra, R. Insights into the CO_2 capture over amine-functionalized mesoporous silica adsorbents derived from rice husk ash. *J. Environ. Chem. Eng.* **2020**, *8*, 104362. [CrossRef]